A lung-on-chip model reveals an essential role for alveolar epithelial cells in controlling bacterial growth during early tuberculosis

Authors: Vivek V. Thacker[1*], Neeraj Dhar[1], Kunal Sharma[1], Riccardo Barrile[2,3],

Katia Karalis[2], John D. McKinney[1*]

Affiliations:

[1]School of Life Sciences, Swiss Federal Institute of Technology Lausanne (EPFL),

1015 Lausanne, Switzerland.

[2]Emulate Inc, Boston, MA 02210 United States

[3]Present address: University of Cincinnati, USA.

*Correspondence to: vivekvthacker@gmail.com or john.mckinney@epfl.ch

1   **Abstract**

2   *Mycobacterium tuberculosis* (Mtb) makes 'first contact' with a host in the alveolar space, an

3   interaction largely inaccessible to experimental observation. We establish a lung-on-chip model

4   for early tuberculosis and use time-lapse imaging to reveal the dynamics of host-Mtb interactions

5   at an air-liquid interface with a spatiotemporal resolution unattainable in animal models. By

6   reconstituting host physiology in a modular manner, we probe the role of pulmonary surfactant

7   secreted by alveolar epithelial cells (AECs) in early infection. This is difficult to study directly in

8   animal models, as surfactant-deficient animals are either non-viable or develop acute lung

9   pathologies. We demonstrate that surfactant deficiency results in rapid and uncontrolled Mtb

10   growth in both macrophages and AECs. In contrast, under normal surfactant levels, a significant

11   fraction of intracellular bacteria are non-growing. The surfactant-deficient phenotype is rescued

12   by exogenous addition of surfactant replacement formulations, which have no effect on bacterial

13   viability in the absence of host cells. Surfactant partially removes virulence-associated lipids and

14   proteins [1,2] from the bacterial cell surface and consistent with this mechanism of action, we show

15   that attenuation of bacteria lacking the virulence-associated ESX-1 secretion system is independent

16   of surfactant levels. These findings may partly explain why individuals with compromised

17   surfactant function, such as smokers and elderly persons, are at increased risk of developing active

18   tuberculosis.

19

20   **Introduction**

21   Early tuberculosis (TB), a respiratory infection caused by *Mycobacterium tuberculosis* (Mtb) is

22   strongly influenced by host physiology; due to the small diameter of respiratory bronchioles only

23   the smallest aerosol droplets containing 1-2 bacilli are successfully transported to the alveolar

24   space [3] and the 'first contact' with a naïve host is by default a single-cell interaction between an

25   Mtb bacillus and a host cell. There is some evidence that pulmonary surfactant plays host-

26   protective role in these early interactions, but a complete understanding of the role of surfactant is

27   difficult to obtain from animal infection models owing to the lethality of surfactant deficiency. In

28   addition, experiments in animal models [4] cannot provide information about the dynamics of host-

29   Mtb interactions at this early stage with sufficient spatiotemporal resolution [5,6]. A commonly-used

30   *in vitro* model, infection of macrophages with Mtb [7], has been used to probe the role of certain

31   surfactant components, but these studies cannot address the role of native surfactant secreted by

32   AECs at an air-liquid interface (ALI), a condition that has been reported to alter Mtb physiology

33   [8].

34   Organ-on-chip systems recreate tissue-level complexity in a modular fashion, allowing the number

35   of cellular components, their identity, and environmental complexity to be tailored to mimic key

36   aspects of the relevant physiology, such as an ALI in a lung-on-chip (LoC) [9]. These systems have

37   emerged as crucial tools for the replacement of animal models in drug development, toxicity

38   testing, and personalised medicine [10,11]. A far less-explored line of enquiry has been to use them

39   as models to study the dynamics of host-pathogen interactions in a realistic physiological setting

40   [12], where they can combine key advantages of both simpler *in vitro* models and animal models [13].

41   Here, we develop a LoC model of early TB infection and use time-lapse microscopy to study the

42   infection dynamics for AECs and macrophages as independent sites of first contact, and the impact

43   of surfactant on infection of AECs and macrophages under ALI conditions that mimic the alveolar

44   environment *in vivo*.

45

46   **Lung-on-chip model of early tuberculosis**

3

47 Freshly isolated mouse AECs comprise a mix of type I cells (Fig. 1A) and type II cells that produce

48 normal surfactant (NS) levels (Fig. 1B). Prolonged *in vitro* passage causes AECs to adopt a

49 phenotype with deficient surfactant (DS) levels (Fig. 1C), reduced expression of type I and type II

50 markers (Fig. 1D), and fewer and smaller lamellar bodies (Fig. 1E, F). We reconstituted a LoC

51 with confluent monolayers of NS or DS AECs (Fig. 1H) and endothelial cells (Fig. 1I) on opposite

52 faces of a porous membrane (Fig. 1J) and an ALI mimicking the alveolar environment.

53 Macrophages added to the epithelial face may remain there or transmigrate across the membrane

54 to the endothelial (Fig. 1H-J). These cells are obtained from a GFP-expressing mouse strain that

55 enables identification during live-cell microscopy. Importantly, NS and DS AECs maintain these

56 phenotypes on-chip at the ALI (Fig. 1K, L), which enables a direct study of the role of AEC-

57 secreted pulmonary surfactant in early infection. Although the ALI significantly degrades axial

58 resolution and signal-to-noise ratios, we are nonetheless able to identify and track individual

59 infected cells over time. Inoculation of the LoC with between 200 and 800 Mtb bacilli led to

60 infection of both macrophages (white boxes in Fig. 1M, P, zooms in Fig. 1O, R) and AECs (yellow

61 boxes in Fig. 1M, P, zooms in Fig. 1N,Q) under both NS (Fig.1M-O) and DS (Fig. 1P-R)

62 conditions. Although the current paradigm in TB focuses on macrophage infection, examination

63 of Mtb-infected cells isolated from the lungs of a mouse at 8 days post infection revealed that 7.3%

64 of infected cells (n = 163) were CD45- pro-SPC+ type II AECs (Fig. S1A-C); we did not find

65 instances of type I AEC infection. The LoC model faithfully reproduces AEC infection, albeit at

66 a higher frequency (Fig. S1D). This in turn enables us to study the infection dynamics in AECs

67 and macrophages simultaneously.

68

69 **Surfactant deficiency leads to uncontrolled intracellular growth of Mtb**

4

70   We used time-lapse microscopy to quantify the intracellular growth of Mtb by measuring the total

71   fluorescence intensity of single infected cells over time (Fig. 2). Between 3 and 5 days post-

72   infection under NS (Fig. 2, A-D, Movie S1) or DS (Fig. 2, E-H, Movie S2) conditions, intracellular

73   growth of Mtb is highly variable in both AECs (Fig. 2I, K) and macrophages (Fig. 2J, L). Plots of

74   the logarithm of total bacterial fluorescence intensity over time for individual infected cells

75   (representing the spread in growth rates) indicate that bacterial growth is exponential in AECs

76   (Fig. 2I, K) and macrophages (Fig. 2J, L). However, under NS conditions, we identified both a

77   substantial "non-growing fraction" (NGF) of bacteria that show very slow growth (doubling time

78   > 168 hours) or even a decrease in fluorescence intensity over time. Intracellular bacterial growth

79   is slower in macrophages compared to AECs under NS conditions but growth rates in both cell

80   types are equivalent under DS conditions (Fig. 2M). Compared to bacterial growth in axenic

81   cultures, growth in both cell types is slower under NS conditions (Fig. S2A) but significantly *faster*

82   under DS conditions (Fig. S2B). Interestingly, there is a much larger spread in growth rates and a

83   small fraction of bacteria continue to grow rapidly even under NS conditions. We observed no

84   spatial pattern of intracellular Mtb growth rates within the lung-on-chip in both NS and DS

85   conditions, confirming that the observed distributions of growth rates are not due to spatial

86   heterogeneity within the device (Fig. S3A, B). Taken together these results suggest that surfactant

87   deficiency shifts the host-pathogen equilibrium in favour of Mtb, resulting in uncontrolled

88   bacterial growth even in macrophages.

89

90   **Exogenous addition of surfactant restores control of Mtb growth**

91   Although reduced surfactant secretion in DS LoCs correlates with increased Mtb replication, this

92   shift could reflect other physiological changes that occur during *in vitro* passage of AECs. We

5

93   therefore asked whether uncontrolled intracellular replication of Mtb in LoCs reconstituted with

94   DS AECs could be rescued by exogenous addition of surfactant. A 1% solution of Curosurf^{TM}, a

95   pulmonary surfactant formulation comprising dipalmitoylphospatidylcholine (DPPC) and the

96   hydrophobic surfactant proteins SP-B and SP-C, was used to treat either Mtb or the DS LoC prior

97   to infection. Both procedures attenuated intracellular Mtb growth and generated a non-growing

98   fraction similar in magnitude to infected NS LoCs (Fig. 2N, Table S1). Curosurf^{TM} treatment does

99   not affect Mtb viability *in vitro* in the absence of host cells (Fig. S4), suggesting that surfactant

100   protects by altering the interaction of Mtb with host cells rather than by any direct effect on

101   bacterial physiology. We conclude that uncontrolled intracellular growth of Mtb in DS LoCs is

102   largely attributable to reduced surfactant secretion.

103

104   **Attenuation of an ESX-1 deficient strain of Mtb is independent of surfactant**

105   We examined whether Mtb mutants that were previously shown to be attenuated in the mouse

106   model of tuberculosis are also attenuated in the LoC model and whether surfactant plays a role in

107   attenuation. Mtb lacking the isocitrate lyase genes *icl1* and *icl2* grows normally under standard

108   conditions *in vitro* but is incapable of growth in the lungs of mice and is rapidly cleared [14]. In the

109   LoC model, we found that the Δ*icl1* Δ*icl2* strain is unable to grow in either AECs or macrophages

110   even under the more-permissive DS conditions (Fig. 3C, S5 A-C), indicating that attenuation of

111   this mutant is similar in the LoC and mouse models and independent of surfactant.

112

113   The activity of the ESX-1 Type VII secretion system, a major Mtb virulence factor that is required

114   for escape from the phagosome into the cytosol [15], is upregulated during AEC infection[16]. In

115   comparison to wild-type Mtb, whose intracellular growth rate is strongly dependent on surfactant

6

116   levels (Fig. 3D-G), intracellular growth of an ESX-1 deficient strain (5'Tn::*pe35* strain [17]) is

117   largely independent of surfactant levels (Fig. 3H-K) and remains attenuated even under DS

118   conditions.   Macrophages are less permissive than AECs for intracellular growth of ESX-1

119   deficient Mtb under both NS and DS conditions (Fig. S6C, D), in contrast to wild-type Mtb, which

120   grows more slowly in macrophages than in AECs under NS but not DS conditions (Fig. S6A,B).

121   Thus, attenuation of ESX-1 deficient bacteria is not rescued by surfactant deficiency. This

122   demonstrates that ESX-1 secretion is necessary for rapid intracellular growth in the absence of

123   surfactant, consistent with the hypothesis that surfactant may attenuate Mtb growth by depleting

124   ESX-1 components on the bacterial cell surface [2].

125

126   Curosurf[TM] binds to the Mtb cell surface and removes virulence-associated lipids

127   Although attenuation of the ESX-1 deficient strain is completely independent of surfactant in

128   AECs (Fig. 3H, I), surfactant still has a small but significant impact on growth of ESX-1 deficient

129   Mtb in macrophages (Fig. 3J, K).   We therefore hypothesized that an additional mechanism of

130   surfactant-dependent protection could be the removal of virulence-associated lipids from the Mtb

131   cell surface.   Consistent with this idea, microscopic examination of Mtb exposed to fluorescently

132   labelled Curosurf[TM] revealed that surfactant readily coated the bacteria (Fig. 3L, M, S7), albeit

133   heterogeneously (compare Fig, S7A, B with Fig. S7C, D).   We also examined the effect of

134   surfactant on the composition of the Mtb cell surface by comparing the total cell-associated lipids

135   and the free (released) lipids prepared from untreated and Curosurf[TM]-treated Mtb.   We found that

136   Curosurf[TM] partially strips the Mtb cell surface of sulfoglycolipids (SGL) (Fig. 3N, P) and

137   trehalose dimycolate (TDM) (Fig. 3O, P), but not phthiocerol dimycocerosates (PDIM) (Fig. S8).

7

138   The surfactant-mediated removal of these virulence-associated lipids[1] suggests an additional

139   mechanism for the attenuation of intracellular growth of Mtb in macrophages.

140

141   **Discussion**

142   AECs are the major cellular component of the distal lung, yet despite sporadic reports of AEC

143   infection in human tuberculosis [18,19], the role of AECs remains controversial. Previous work has

144   revealed the specific role of hydrophilic SP-A and SP-D proteins [20,21] and surfactant hydrolase

145   enzymes [22,23] on host-Mtb interactions. In contrast, in the LoC model of early tuberculosis

146   presented here, secretion of native surfactant by AECs at an air-liquid interface (ALI) can be

147   modulated. This physiological perturbation, which cannot be achieved in animal models due to

148   the lethality of surfactant deficiency, provides a comprehensive view of the role of AECs in early

149   tuberculosis and is an important advance over previous co-culture models for TB [24–26]. The

150   unexpectedly rapid and uncontrolled intracellular growth of Mtb at the ALI in the absence of

151   surfactant has not been reported previously in simpler *in vitro* models of host cell infection. Under

152   NS conditions we identified a substantial non-growing fraction of intracellular Mtb in both AECs

153   and macrophages, which may be equivalent to the "non-growing but metabolically active"

154   (NGMA) populations previously observed in the lungs of mice [27]. These examples underscore

155   some of the advantages of the LoC model, which provides a more faithful mimesis of the complex

156   *in vivo* environment compared to conventional *in vitro* models.

157

158   Taken together, our findings indicate that pulmonary surfactant plays on important role in host

159   innate immunity during early Mtb infection, which may partly explain why individuals with

160   defective surfactant function [28–30] also show an increased risk of developing active TB. We also

161   report that AECs are more permissive to Mtb growth than macrophages under NS (but not DS)

162   conditions. Infection of AECs is not an artefact of the LoC model, as we also identified infected

163   AECs in the lungs of aerosol-infected mice using a sensitive microscopy-based approach, which

164   might be more discriminating than FACS-based approaches used previously [31]. Alveolar

165   macrophages in the lung have been shown to be sessile [5], and so the higher incidence of AEC

166   infection in the LoC model is probably due to differences in the method of Mtb inoculation. This

167   in turn suggests a deeper link between the airway and alveolar geometries that determine aerosol

168   deposition in the lungs (which are not captured in the LoC model but could be addressed with 3D

169   bioprinted models [32]) and resident lung immunity. Given the very low inoculum size in human

170   Mtb (most infected individuals harbour just one primary lesion originating from a single bacillus

171   [33], we speculate that first contact with an AEC, albeit much rarer *in vivo* could potentially lead to

172   a more aggressive infection. This could provide one explanation for the observation that the

173   proportion of exposed individuals who develop clinical tuberculosis is low.

174

175   Time-lapse imaging at an ALI in the LoC infection model directly quantifies bacterial growth rates

176   with a spatiotemporal resolution that is unachievable using indirect measurements of bacterial

177   growth rates in mouse models of tuberculosis (e.g., plating tissue homogenates to measure colony

178   forming units). The deliberate choice to use murine over human cells allows us to add macrophages

179   to the chip from a mouse line that constitutively expresses GFP, which allows unambiguous

180   identification of these cells over days and is superior to the use of CellTrackerTM and other

181   fluorescent dyes. It also enables us to benchmark the model with previous reports from the mouse

182   model for TB. For example, average growth rates for wild-type Mtb under NS conditions are in

183   good agreement with net Mtb growth rates measured using a plasmid-loss assay in mice

9

184   (Supplementary Discussion) [34].   However, our microscopy-based approach also reveals the

185   population distribution of growth rates, which highlights that even under NS conditions, a small

186   proportion of cells show robust intracellular Mtb growth, and that robust and attenuated Mtb

187   growth can occur in close proximity to each other on-chip. These observations reinforce an

188   important role for cell-to-cell heterogeneity in host-Mtb outcomes [35].   The growth characteristics

189   of ESX-1 deficient Mtb in our LoC model are also in good agreement with experiments from

190   animal models, further validating the LoC model (Supplementary Discussion; Fig S9).

191

192   Exogenous addition of Curosurf[TM], a surfactant replacement formulation of phospholipids and

193   hydrophobic proteins, rescues the effects of surfactant deficiency on mycobacterial growth.

194   Phospholipids are the main component of native surfactant, and lipid recycling is a key function

195   of type II AECs and alveolar macrophages [36].   The two-way interaction of surfactant with the

196   bacterial cell surface (surfactant removes virulence-associated Mtb surface lipids and proteins, and

197   surfactant lipids coat the Mtb surface) may alter how host cells take up these bacteria, or how they

198   are processed after uptake.   More generally, surfactant phospholipids have been shown to have

199   antiviral properties, and can serve as a potent adjuvant for antiviral vaccines either on their own [37]

200   or as a medium for delivery of immune-stimulating molecules to AECs [38].   Our findings suggest a

201   potential role for pulmonary surfactant replacement formulations in host-directed therapies against

202   tuberculosis.   These insights were made possible by use of an organ-on-chip system that

203   reproduces host physiology in a modular and tuneable fashion, which is frequently impossible to

204   achieve *in vivo*.

205   **Methods**

206   A detailed experimental protocol for the establishment of the lung-on-chip infection model, a

207   description of the characterization of AECs via qRT-PCR, protocols for live-cell imaging and

208   analyses for quantification of Mtb growth are included in the Materials and Methods in the

209   Supplementary Information. The Materials and Methods also includes an overview of the

210   procedures for the infection of mice with Mtb, generation of single-cell suspension from lungs,

211   and the labelling strategies used to identify infected AECs and immune cells. The Supplementary

212   Information also includes two additional sections of Supplementary Discussion that compare the

213   intracellular growth rate measurements from the lung-on-chip model with those from a plasmid

214   rate-loss assay, and use the growth rate measurements to model the relative attenuation of the ESX-

215   1 mutant versus WT observed using colony forming unit assays.

216   **Materials and Methods**

217   <u>Cell culture</u>

218   Primary C57BL/6 alveolar epithelial cells (AECs) and lung microvascular endothelial cells were

219   obtained from Cell Biologics, USA. Each vial of AECs consisted of a mix of Type I and Type II

220   AECs, which was verified both by immunostaining and qRT-PCR for type I and type II markers

221   (Fig. 1A-C). Both cell types were cultured *in vitro* in complete medium comprising base medium

222   and supplements (Cell Biologics, USA) in 5% CO_2 at 37°C. Normal surfactant (NS) AECs were

223   seeded directly on the lung-on-chip (see below), without prior *in vitro* culture. Deficient surfactant

224   (DS) AECs were passaged 6-11 times before use.

225

226   <u>Bone marrow isolation and culture</u>

227   Bone marrow was obtained from 6-8-week-old Tg(act-EGFP) Y01Osb mice (Jackson

228   Laboratories, USA, Stock Number 006567) and cryopreserved. This transgenic line constitutively

229   expresses enhanced GFP under the control of the chicken beta-actin promoter and the

230   cytomegalovirus enhancer. Mice were housed in a specific pathogen-free facility. Animal

231   protocols were reviewed and approved by EPFL's Chief Veterinarian, by the Service de la

232   Consommation et des Affaires Vétérinaires of the Canton of Vaud, and by the Swiss Office

11

233   Vétérinaire Fédéral. Bone marrow was cultured in Dulbecco's Modified Eagle Medium (DMEM)

234   (Gibco) supplemented with 10% fetal bovine serum (FBS, Gibco) and differentiated for 7 days

235   with 20 ng/ml recombinant murine Macrophage-Colony Stimulating Factor protein (M-CSF)

236   (Thermo Fisher Scientific). Bone marrow was cultured in plastic petri dishes without pre-

237   sterilisation (Greiner Bio-one) so that differentiated macrophages could be detached. No

238   antibiotics were used in the cell culture media for all cell types to avoid activation of macrophages

239   or inhibition of Mtb growth.

240

241   <u>Quantitative Real-Time PCR (qRT-PCR)</u>

242   Freshly isolated AECs (NS) were grown overnight in cell-culture microdishes (Ibidi) or T-25 cell

243   culture flask (TPP, Switzerland). Passaged AECs (DS) were grown to confluency in a T-75 cell

244   culture flask (TPP). Growth media was removed from the flask, and the cells were incubated with

245   the appropriate volume of TRIzol (Ambion) as per the manufacturer's instruction. TRIzol-treated

246   cell lysates were stored at -20°C before further processing. RNA was precipitated with

247   isopropanol, washed in 75% ethanol, resuspended in 50 µl of DEPC-treated water, treated with

248   Turbo DNase (Ambion), and stored at -80°C until use. DNase-treated RNA was used to generate

249   cDNA using the SuperScript®II First-Strand Synthesis System with random hexamers

250   (Invitrogen), which was stored at -20°C. Specific primers for *gadph*, *sftpc*, *abca3*, and *aqp5* are

251   listed in Table S2. qRT-PCR reactions were prepared with SYBR®Green PCR Master Mix

252   (Applied Biosystems) with 1 µM primers, and 2 µl cDNA. Reactions were run as absolute

253   quantification on ABI PRISM®7900HT Sequence Detection System (Applied Biosystems).

254   Amplicon specificity was confirmed by melting-curve analysis.

255

256   <u>AEC characterization via immunofluorescence</u>

257   Freshly isolated AECs (NS) or passaged AECs (DS) were grown overnight in 35 mm cell-culture

258   microdishes (Ibidi GmbH, Germany). The confluent layer of cells was subsequently fixed with

259   2% paraformaldehyde (Thermo Fisher Scientific) in phosphate-buffered saline (PBS, Gibco) at

260   room temperature for 30 minutes, washed with PBS, and incubated with a blocking solution of 2%

261   bovine serum albumin (BSA) in PBS for 1 hour at room temperature. The blocking solution was

262   removed and the cells were incubated with the primary antibody (1:100 dilution in 2% BSA

263   solution in PBS) overnight at 4°C. Antibodies used were anti-Podoplanin Monoclonal Antibody

264   (eBio8.1.1 (8.1.1)), Alexa Fluor 488, eBioscience™ (ThermoFisher Scientific), and anti-pro-SPC

265   antibody (ab40879, Abcam). The cell-culture microdishes were washed 3x in PBS, incubated with

266   a fluorescent secondary antibody (Donkey anti rabbit Alexa Fluor 568 (A10042 Thermo Fisher)

267   in a solution of 2% BSA in PBS for 1 hour at room temperature, then thoroughly washed with PBS

268   and incubated with Hoechst 33342 nuclear staining dye (1:1000 dilution, Thermo Fisher Scientific)

269   for 15-20 minutes for nuclear staining. Confocal images were obtained on a Leica SP8 microscope

270   in the inverted optical configuration.

271

272   <u>Bacterial culture</u>

273   All bacterial strains were derived from *Mycobacterium tuberculosis* strain Erdman and cultured at

274   37°C.   Liquid medium: Middlebrook 7H9 (Difco) supplemented with 0.5% albumin, 0.2%

275   glucose, 0.085% NaCl, 0.5% glycerol, and 0.02% Tyloxapol. Solid medium: Middlebrook 7H11

276   (Difco) supplemented with 10% OADC enrichment (Becton Dickinson) and 0.5% glycerol.

277   Aliquots were stored in 15% glycerol at -80°C and used once. All strains were transformed with

278   a plasmid integrated at the chromosomal *attB* site to allow constitutive expression of the

279   fluorescent protein tdTomato under the control of the hsp60 promoter. Wild-type (WT) refers to

280   the Erdman strain constitutively expressing tdTomato. The 5'Tn::*pe35* (ESX-1 deficient) strain

281   was generated using transposon mutagenesis [1].

282

283   <u>Infection of mice with Mtb</u>

284   Female C57BL/6 mice (Charles River Laboratories) were housed in a specific pathogen-free

285   facility. Animal protocols were reviewed and approved by EPFL's Chief Veterinarian, by the

286   Service de la Consommation et des Affaires Vétérinaires of the Canton of Vaud, and by the Swiss

287   Office Vétérinaire Fédéral. Mice were infected by the aerosol route using a custom-built aerosol

288   machine, as described [2]. Bacteria were grown to exponential phase, corresponding to an optical

289   density at 600 nm (OD_{600}) of 0.5, collected by centrifugation at 2850 g for 10 minutes, and

290   resuspended in PBS supplemented with 0.05% Tween 80 (PBS-T). The bacterial suspension was

291   subjected to low-speed centrifugation (700 g) for 5 minutes to remove bacterial aggregates. The

292   cell suspension was adjusted to OD_{600} 0.1 with PBS-T in a final volume of 20 ml, which was used

293   to infect mice by aerosol. At 1 day post-infection, a group of 4 mice were euthanized by CO_2

294   overdose; the lungs were removed aseptically and homogenised in 3 ml of 7H9 medium. Serial

295   dilutions were plated on 7H11 plates containing 100 μg/ml cycloheximide (Sigma) and colonies

296   were counted after 4-5 weeks of incubation at 37°C. The aerosol infection corresponded to a

297   bacterial load of between 60-100 colony-forming units (CFU) per mouse at 1 day post-infection.

298

299   <u>Extraction and quantification of Mtb-infected AECs</u>

300   At 8 days post-infection, a group of 5 mice were euthanized by an overdose of ketamine/xylazine

301   anaesthetic, and the lungs were washed with PBS delivered via injection through the right ventricle

302   of the heart to remove excess red blood cells. Lungs from each mouse were removed aseptically,

303   minced into small pieces with scissors, and added to 2.5 ml of lung dissociation media

304   reconstituted as per the manufacturer's instructions (Lung Dissociation Kit – Mouse, Miltenyi

305   Biotec). The lungs were then dissociated using a gentleMACS Octo Dissociator (Miltenyi Biotec).

306   The resulting homogenate was filtered through a 40 μm cell filter, centrifuged for 10 minutes at

307   300 g, and resuspended in alveolar epithelial cell media supplemented with 10% FBS. The

308   homogenate was then plated in 50 mm glass-bottom cell-culture dishes (Ibidi) and incubated for

309   36-48 hours to allow for epithelial cell attachment. Additional medium was added to each cell-

310   culture dish at 24 hours. The cells were subsequently fixed with paraformaldehyde and stained for

311   immunofluorescence as already described. Antibodies: anti-Podoplanin Monoclonal Antibody

312   (eBio8.1.1 (8.1.1)), Alexa Fluor 488, eBioscience™ (ThermoFisher Scientific) to label Type I

313   AECs, anti-pro-SPC antibody (ab40879, Abcam) followed by secondary antibody staining

314   (Donkey anti rabbit Alexa Fluor 488 (A21206 Thermo Fisher)) to label Type II AECs, and Alexa

315   647 anti-CD45 antibody (103124, BioLegend).

316

317   <u>Murine lung-on-chip (LoC) model</u>

318   LoC made of polydimethylsiloxane (PDMS) were obtained from Emulate (Boston, USA).

319   Extracellular matrix (ECM) coating was performed as per the manufacturer's instructions. Chips

320   were activated using ER-1 solution (Emulate) dissolved in ER-2 solution at 0.5 mg/ml (Emulate)

321   and exposed for 20 minutes under UV light. The chip was then rinsed with coating solution and

322   exposed again to UV light for a further 20 minutes. Chips were then washed thoroughly with PBS

323   before incubating with an ECM solution of 150 μg/ml bovine collagen type I (AteloCell, Japan)

324   and 30 μg/ml fibronectin from human plasma (Sigma-Aldrich) in PBS buffered with 15 mM

325   HEPES solution (Gibco) for 1-2 hours at 37°C. If not used directly, coated chips were stored at

14

326   4°C and pre-activated before use by incubation for 30 minutes with the same ECM solution at

327   37°C. Endothelial cells were cultured overnight at 37°C and 5% CO_2 in T-75 cell culture flasks,

328   detached with 0.05% Trypsin, concentrated to 5-10 million cells/ml, and seeded on the bottom

329   face of the PDMS membrane. The chip was then incubated for a short period at 37°C to allow the

330   endothelial cells to spread and subsequently seeded with AECs. Freshly isolated AECs were

331   seeded directly from cryopreserved vials received from the supplier. while DS LoCs were seeded

332   from cells cultured overnight at 37°C and 5% CO_2, in both cases at a concentration of 1-2 million

333   cells/ml. The chip was incubated overnight with complete epithelial and endothelial media in the

334   epithelial and endothelial channels, respectively, under static conditions. The next day, the chip

335   was washed and a reduced medium for the air-liquid interface (ALI) was flowed through the

336   vascular channel using syringe pumps (Aladdin-220, Word Precision Instruments) at 60 μl/hour

337   as described [3]. The composition of the ALI media used was as described in [3] but with an FBS

338   concentration of 5%. The epithelial face was incubated with epithelial base medium with 200 nM

339   dexamethasone (Sigma Aldrich) without FBS supplementation. Flow was maintained over 2-3

340   days with daily replacement of the medium on the epithelial face (with dexamethasone

341   supplementation). At the end of this period, GFP-expressing macrophages differentiated for 7 days

342   in M-CSF (described above) were detached from the petri dish using 2 mM

343   ethylenediaminetetraacetic acid (EDTA, Sigma Aldrich) in PBS at 4°C, centrifuged at 300 g for 5

344   minutes, and resuspended in a small volume of epithelial cell media without dexamethasone. This

345   solution containing macrophages was introduced onto the epithelial face and incubated for 30

346   minutes at 37°C and 5% CO_2 to allow macrophages to attach to the epithelial cells. Medium on

347   the epithelial face was then removed and the chip was maintained overnight at an air-liquid

348   interface (ALI). Chips that successfully maintained the ALI overnight were transferred to the

349   biosafety level 3 (BSL-3) facility for Mtb infection. No antibiotics were used in any of the cell

350   culture media for setting up the LoC model.

351

352   Immunostaining of uninfected LoCs

353   Uninfected LoCs were maintained at an ALI for up to 7 days after addition of macrophages, during

354   which time ALI medium was flowed through the endothelial channel at 60 μl/hour. After 7 days

355   at the ALI, the chip was fixed for immunostaining as described above; a permeabilization step

356   with a solution containing 2% w/v saponin (Sigma Aldrich) and 0.1% Triton X-100 (Sigma

15

357   Aldrich) was performed before incubation with the secondary antibody. F-actin on both the

358   epithelial and endothelial face was stained using Sir-Actin dye (Spherochrome) at 1 μM for 30

359   minutes concurrently with Hoechst staining, as described above.

360

361   Infection of the LoC with Mtb

362   The chip was assembled into a stage top incubator (Okolab, Italy) prior to infection and flow of

363   medium through the vascular channel was maintained throughout the course of the experiment by

364   use of a syringe pump. A 1 ml aliquot of a culture of Mtb grown to exponential phase (OD_{600} 0.3-

365   0.5) was centrifuged at 5000 g for 5 minutes at room temperature, the supernatant was removed,

366   and the cell pellet was resuspended in 200 μl of epithelial cell media without FBS. A single-cell

367   suspension was generated via filtration through a 5 μm syringe filter (Millipore). The single-cell

368   suspension was diluted 100-fold in epithelial media and 30 μl was added to the epithelial channel

369   of the LoC. The infectious dose was measured by plating serial dilutions of the single-cell

370   suspension on 7H11 plates and counting CFU after 3-4 weeks of incubation at 37°C, and varied

371   between 200 and 800 Mtb bacilli. The chip was incubated for 2-3 hours at 37°C and 5% CO_2 to

372   allow Mtb infection of cells on the epithelial face, after which the solution on the epithelial face

373   was withdrawn. The proportion of bacteria that remained on the chip was estimated by plating

374   serial dilutions of the withdrawn solution on 7H11 plates and counting CFU after 3-4 weeks of

375   incubation at 37°C. The epithelial face was returned to ALI and the inlets of the infected chip

376   were sealed with solid pins as a safety precaution for time-lapse microscopy imaging in the BSL-

377   3 facility.

378

379   Time-lapse microscopy of the Mtb-infected LoC

380   The LoC was placed in a microscope stage-top incubator and mounted on the stage of a widefield

381   Nikon Ti-2 microscope. The stage-top incubator was connected to a gas mixer (Okolab) to

382   maintain 5% CO_2 throughout the imaging period. Flow of medium through the vascular channel

383   was maintained throughout this period via the use of a syringe pump. The chip was imaged using

384   a long working distance 20x phase-contrast objective (NA=0.75, Ph2, Nikon) at 1.5-hour or 2-

385   hour imaging intervals. The epithelial face of the chip (where the refractive index differences were

386   highest due to the ALI) was maintained in focus using the Nikon Perfect Focus System. At each

387   timepoint, a Z-stack of 9-10 images with an axial spacing of 10 μm was taken series for a series

16

388 of fields of view along the length of the chip to account for the dynamic 3D movement of

389 macrophages between both faces, as well as drift in focus over time. Each field of view was ~660

390 x 600 μm^2. Using a Sola SE II light source (Lumencor, USA), macrophages and Mtb were

391 identified through fluorescence emission in the green (macrophages) and red (Mtb) channels using

392 GFPHQ and mcherryHQ 32 mm dichroic filters, respectively. Phase-contrast images were also

393 captured; the poor quality of these images due to the refractive index differences at the ALI serves

394 as a continuous verification that ALI is maintained. All images were captured with an EMCCD

395 camera (iXON Ultra 888, Andor) cooled to -65°C, with an EM gain setting of 300 to allow the

396 sample to be illuminated with a low intensity of incident light in all fluorescent channels with

397 reduced photodamage. Co-localization of the green and red fluorescence signals over a time

398 course was identified as consistent with macrophage infection. Bacteria that did not co-localize

399 with macrophages over time were assumed to infect AECs, which was verified by subsequent

400 immunostaining.

401

402 <u>Data analysis</u>

403 Images were visualized using ImageJ. Macrophage and AEC infections from each field of view

404 were visually curated by assessing the co-localization of fluorescent signals over time. Smaller

405 stacks of 1-2 microcolonies were assembled. Custom-written software in MATLAB was used to

406 measure the total fluorescence intensity of each intracellular bacterial microcolony which used the

407 nestedSortStruct algorithm for MATLAB (https://www.github.com/hugheylab/nestedSortStruct,

408 GitHub) written by the Hughey lab. Briefly, at each timepoint, the Z-stack with the highest

409 intensity in the fluorescence channel was identified; this image was then segmented to identify the

410 bacterial microcolony; total fluorescence was measured by summing the intensity of all the pixels

411 in this region after subtracting a value for each pixel that represented the average background

412 fluorescence. We chose to measure the total fluorescence intensity because it accounts for both

413 bacterial growth and dilution of the fluorescent protein due to growth (which is slow in a slow-

414 growing bacterium like Mtb). We were unable to measure microcolony volumes accurately using

415 widefield imaging due to poor axial resolution caused by large refractive index differences at the

416 ALI; therefore, we obtained this value from only the Z stack with the highest intensity. Statistical

417 analysis was performed using Origin 9.2 (OriginLabs) and p-values were calculated using a

17

418 Kruskal-Wallis one-way ANOVA test, with the null hypothesis that the medians of each
419 population were equal.

420

421 Simulations of *in vivo* infections

422 Growth rate datasets for wild-type and ESX-1 deficient strains of Mtb in NS and DS LoC
423 conditions were fitted with a non-parametric Kernel Smoothed distribution. We simulated a low-
424 dose aerosol infection of 50 bacteria in the alveolar space of n=100 or n=1000 mice, and
425 conservatively assumed that every bacterium interacted with a macrophage upon first contact.
426 Each bacterium was assigned a growth rate picked at random from the Kernel Smoothed
427 distributions and assumed to grow exponentially with these growth rates to generate an
428 intracellular microcolony. The total bacterial numbers in each mouse at 2, 3, 5, 7 and 14 days
429 post-infection were obtained by summing the bacterial counts from each microcolony for each
430 mouse and are shown in Fig. S9E-G. Total bacterial numbers for n=100 mice of WT and ESX-1
431 deficient strains are shown in Fig. S9.

432

433 Curosurf^{TM} treatment of DS LoCs

434 Curosurf^{TM} (Chiesi Pharmaceuticals, Italy) was used as a 1% solution in epithelial medium for all
435 LoC experiments. In the case where Curosurf^{TM} was added to a DS LoC, a 1% solution was
436 introduced to the epithelial face after the macrophages were added but before ALI was introduced
437 for 2 minutes, and then removed. The following morning, this procedure was repeated just prior
438 to the addition of the single-cell suspension of Mtb in the manner described above. Alternatively,
439 a 1 ml aliquot of Mtb in exponential phase in 7H9 media was centrifuged at 5000 g for 5 minutes,
440 resuspended in 1 ml of cell culture media containing 1% Curosurf^{TM,} and incubated for 10-15
441 minutes at room temperature. This solution was then centrifuged again at 5000 g for 5 minutes
442 and a single-cell suspension of Mtb was generated as described above. Fluorescent labelling of
443 surfactant was achieved by adding TopFluor phosphatidylcholine (10% v/v, Avanti Polar Lipids)
444 to Curosurf^{TM} before dilution in cell culture medium.

445

446 Total free lipid extraction and thin-liquid chromatography (TLC)

447 Mtb cultures (10 ml each) were grown to stationary phase in 7H9 with 10 μC_i of ^{14}C-propionate
448 added during exponential phase. Total free lipid extraction from the bacterial pellet, supernatant,

18

449   and supernatant from bacteria pre-treated with 3% Curosurf[TM] for 15 minutes at 37°C were

450   extracted as described [4]. Extracted free lipids were air-dried, resuspended in 2:1 v/v solution of

451   chloroform: methanol, and aliquots were spotted on 5 x 10 cm TLC silica gel 60 F_{254} (Merck).

452   Running solvent was 90:10:1 chloroform: methanol: water for the analysis of sulfoglycolipids

453   (SGL), 80:20:2 chloroform: methanol: ammonium hydroxide for the analysis of trehalose

454   dimycolate (TDM), and 9:1 petroleum ether: diethyl ether for the analysis of pthiocerol

455   dimycocerosates (PDIM) and triacyclglycerols (TAG). The developed TLC plate was exposed to

456   an Amersham Hyperfilm ECl (GE Healthcare) for phosphorescence imaging and visualized with

457   a Typhoon scanner (GE Healthsciences). Intensities of the bands observed were quantified using

458   ImageJ.

459

19

460   **Data availability statement**

461   The datasets generated during and/or analysed during the current study are available from the
462   corresponding authors on reasonable request. Software code used to analyse these datasets will be
463   uploaded to Github prior to publication.
464

Bibliography

1. Dulberger, C. L., Rubin, E. J. & Boutte, C. C. The mycobacterial cell envelope — a moving target. *Nature Reviews Microbiology* vol. 18 47–59 (2020).

2. Raffetseder, J., Iakobachvili, N., Loitto, V., Peters, P. J. & Lerm, M. Retention of EsxA in the Capsule-Like Layer of Mycobacterium tuberculosis Is Associated with Cytotoxicity and Is Counteracted by Lung Surfactant. *Infect. Immun.* **87**, (2019).

3. Ma, B. & Darquenne, C. Aerosol deposition characteristics in distal acinar airways under cyclic breathing conditions. *J. Appl. Physiol.* **110**, 1271–1282 (2011).

4. Collins, F. M. & Orme, I. M. Mouse Model of Tuberculosis. in *Tuberculosis* 113–134 (American Society of Microbiology, 1994). doi:10.1128/9781555818357.ch8.

5. Westphalen, K. *et al.* Sessile alveolar macrophages communicate with alveolar epithelium to modulate immunity. *Nature* **506**, 503–506 (2014).

6. Looney, M. R. *et al.* Stabilized imaging of immune surveillance in the mouse lung. *Nat. Methods* **8**, 91–96 (2011).

7. Lerner, T. R. *et al.* Mycobacterium tuberculosis replicates within necrotic human macrophages. *J. Cell Biol.* (2017).

8. Ojha, A. K. *et al.* Growth of *Mycobacterium tuberculosis* biofilms containing free mycolic acids and harbouring drug-tolerant bacteria. *Mol. Microbiol.* **69**, 164–174 (2008).

9. Huh, D. *et al.* Reconstituting organ-level lung functions on a chip. *Science* **328**, 1662–8 (2010).

10. Ghaemmaghami, A. M., Hancock, M. J., Harrington, H., Kaji, H. & Khademhosseini, A. Biomimetic tissues on a chip for drug discovery. *Drug Discov. Today* **17**, 173–81 (2012).

11. Ronaldson-Bouchard, K. & Vunjak-Novakovic, G. Organs-on-a-Chip: A Fast Track for Engineered Human Tissues in Drug Development. *Cell Stem Cell* **22**, 310–324 (2018).

12. Grassart, A. *et al.* Bioengineered Human Organ-on-Chip Reveals Intestinal Microenvironment and Mechanical Forces Impacting Shigella Infection. *Cell Host Microbe* **26**, 435-444.e4 (2019).

13. Torrelles, J. B. & Schlesinger, L. S. Integrating Lung Physiology, Immunology, and Tuberculosis. *Trends Microbiol.* **25**, 688–697 (2017).

14. Muñoz-Elías, E. J. & McKinney, J. D. Mycobacterium tuberculosis isocitrate lyases 1 and 2 are jointly required for in vivo growth and virulence. *Nat. Med.* **11**, 638–44 (2005).

15. van der Wel, N. *et al.* M. tuberculosis and M. leprae Translocate from the Phagolysosome

497   to the Cytosol in Myeloid Cells. *Cell* **129**, 1287–1298 (2007).

498   16.   Ryndak, M. B., Singh, K. K., Peng, Z. & Laal, S. Transcriptional Profile of
499   Mycobacterium tuberculosis Replicating in Type II Alveolar Epithelial Cells. *PLoS One*
500   **10**, e0123745 (2015).

501   17.   Chen, J. M. *et al. Mycobacterium tuberculosis* EspB binds phospholipids and mediates
502   EsxA-independent virulence. *Mol. Microbiol.* **89**, 1154–1166 (2013).

503   18.   Barrios-Payán, J. *et al.* Extrapulmonary Locations of Mycobacterium tuberculosis DNA
504   During Latent Infection. *J. Infect. Dis.* **206**, 1194–1205 (2012).

505   19.   Hernández-Pando, R. *et al.* Persistence of DNA from Mycobacterium tuberculosis in
506   superficially normal lung tissue during latent infection. *Lancet* **356**, 2133–2138 (2000).

507   20.   Ferguson, J. S. *et al.* Surfactant protein D increases fusion of Mycobacterium tuberculosis-
508   containing phagosomes with lysosomes in human macrophages. *Infect. Immun.* **74**, 7005–
509   7009 (2006).

510   21.   Pasula, R. *et al.* Surfactant Protein A (SP-A) Mediates Attachment of *Mycobacterium*
511   *tuberculosis* to Murine Alveolar Macrophages. *Am. J. Respir. Cell Mol. Biol.* **17**, 209–217
512   (1997).

513   22.   Scordo, J. M. *et al.* Mycobacterium tuberculosis Cell Wall Fragments Released upon
514   Bacterial Contact with the Human Lung Mucosa Alter the Neutrophil Response to
515   Infection. *Front. Immunol.* **8**, 307 (2017).

516   23.   Arcos, J. *et al.* Human Lung Hydrolases Delineate Mycobacterium tuberculosis –
517   Macrophage Interactions and the Capacity To Control Infection . *J. Immunol.* **187**, 372–
518   381 (2011).

519   24.   Bermudez, L. E., Sangari, F. J., Kolonoski, P., Petrofsky, M. & Goodman, J. The
520   efficiency of the translocation of Mycobacterium tuberculosis across a bilayer of epithelial
521   and endothelial cells as a model of the alveolar wall is a consequence of transport within
522   mononuclear phagocytes and invasion of alveolar epithelial cells. *Infect. Immun.* **70**, 140–
523   6 (2002).

524   25.   Bielecka, M. K. *et al.* A Bioengineered Three-Dimensional Cell Culture Platform
525   Integrated with Microfluidics To Address Antimicrobial Resistance in Tuberculosis. *MBio*
526   **8**, e02073-16 (2017).

527   26.   Parasa, V. R. *et al.* Modeling Mycobacterium tuberculosis early granuloma formation in
528   experimental human lung tissue. *DMM Dis. Model. Mech.* **7**, 281–288 (2014).

529   27.   Manina, G., Dhar, N. & McKinney, J. D. D. Stress and host immunity amplify
530   mycobacterium tuberculosis phenotypic heterogeneity and induce nongrowing
531   metabolically active forms. *Cell Host Microbe* **17**, 32–46 (2015).

22

532   28.   Finley, T. N. & Ladman, A. J. Low Yield of Pulmonary Surfactant in Cigarette Smokers.
533   *N. Engl. J. Med.* **286**, 223–227 (1972).

534   29.   Subramaniam, S. Biochemical and Biophysical Characterization of Pulmonary Surfactant
535   in Rats Exposed Chronically to Cigarette Smoke. *Fundam. Appl. Toxicol.* **27**, 63–69
536   (1995).

537   30.   Moliva, J. I. *et al.* The Lung Mucosa Environment in the Elderly Increases Host
538   Susceptibility to Mycobacterium tuberculosis Infection. *J. Infect. Dis.* **220**, 514–523
539   (2019).

540   31.   Cohen, S. B. *et al.* Alveolar Macrophages Provide an Early Mycobacterium tuberculosis
541   Niche and Initiate Dissemination. *Cell Host Microbe* **24**, 439-446.e4 (2018).

542   32.   Grigoryan, B. *et al.* Multivascular networks and functional intravascular topologies within
543   biocompatible hydrogels. *Science* **364**, 458–464 (2019).

544   33.   Mckinney, J. D., Jacobs, W. R. & Bloom, B. R. 3 Persisting problems in tuberculosis.
545   *Biomed. Res. Reports* **1**, 51–146 (1998).

546   34.   Gill, W. P. *et al.* A replication clock for Mycobacterium tuberculosis. *Nat. Med.* **15**, 211–
547   214 (2009).

548   35.   Lin, P. L. *et al.* Sterilization of granulomas is common in active and latent tuberculosis
549   despite within-host variability in bacterial killing. *Nat. Med.* **20**, 75–9 (2014).

550   36.   Olmeda, B., Martínez-Calle, M. & Pérez-Gil, J. Pulmonary surfactant metabolism in the
551   alveolar airspace: Biogenesis, extracellular conversions, recycling. *Ann. Anat. - Anat.*
552   *Anzeiger* **209**, 78–92 (2017).

553   37.   Kimoto, T. *et al.* Intranasal influenza vaccination using a new synthetic mucosal adjuvant
554   SF-10: Induction of potent local and systemic immunity with balanced Th1 and Th2
555   responses. *Influenza Other Respi. Viruses* **7**, 1218–1226 (2013).

556   38.   Wang, J. *et al.* Pulmonary surfactant–biomimetic nanoparticles potentiate heterosubtypic
557   influenza immunity. *Science (80-.).* **367**, eaau0810 (2020).
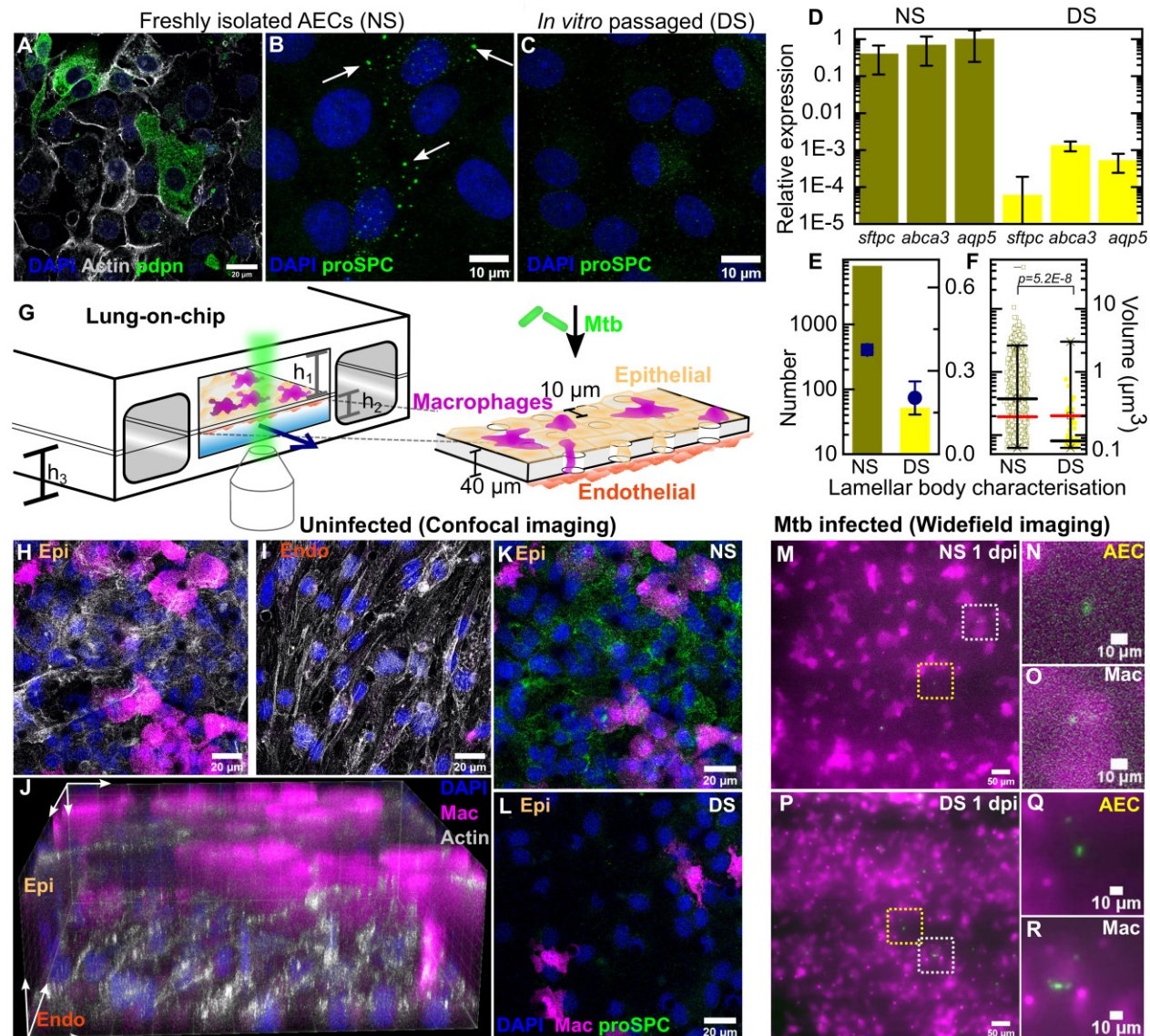558

Fig. 1. Direct observation of the role of pulmonary surfactant in a lung-on-chip model for tuberculosis. Freshly isolated murine alveolar epithelial cells (AECs) are a mixture of (**A**) type I Pdpn-immunostained cells and (**B**) type II pro-SPC-immunostained cells containing lamellar bodies (white arrows). (**C**) *In vitro* passage of AECs generates an intermediate phenotype with (**D**) reduced expression of type II (*sfptc* and *abca3*) and type I (*aqp5*) markers. Error bars represent the standard deviation for two technical repeats for each qPCR. Based on these characteristics we classify these populations as expressing normal surfactant (NS) or deficient surfactant (DS) levels,

24

567   respectively. (**E**) In DS cells, the number and mean volume of pro-SPC+ lamellar bodies is

568   reduced. (**F**) The number of lamellar bodies is also significantly reduced. Mean and median

569   volumes are represented by black and red bars, respectively. Whiskers represent the 1-99 percentile

570   interval. (P = 5.2E-8) (**G**) Schematic of the LoC model of early tuberculosis. Confluent layers of

571   AECs and endothelial cells populate the top and bottom faces of the porous membrane that

572   separates the air-filled "alveolar" (upper) and liquid-filled "vascular" (lower) compartments,

573   creating an air-liquid interface (ALI). GFP-expressing macrophages (magenta) are added to the

574   alveolar compartment to mimic the natural route of infection. h_1 = 1 mm, h_2 = 250 μm, h_3 = 800

575   μm. (**H-I**) Confocal microscope images of an uninfected LoC stained to visualize nuclei (blue),

576   actin (grey), and surfactant (green, anti-pro-SPC antibody) verifies that confluency of epithelial

577   (**H**) and endothelial (**I**) layers is maintained at the ALI over 7 days. 3D imaging reveals occupancy

578   of some pores by macrophages (**J**). LoCs reconstituted with NS (**K**) or DS (**L**) AECs continue to

579   express normal or deficient levels of surfactant, respectively. (**M-R**) Widefield microscope images

580   of LoCs reconstituted with NS (**M-O**) or DS (**P-R**) AECs and infected with a low dose of Mtb

581   expressing td-Tomato (green). Images taken at 1 day post-infection (dpi) show that AECs (yellow

582   boxes (**M, P**) and zooms (**N, Q**)) as well as macrophages (white boxes (**M, P**) and zooms (**O, R**))

583   can be sites of first contact. *P*-values were calculated using a Kruskal-Wallis one-way ANOVA
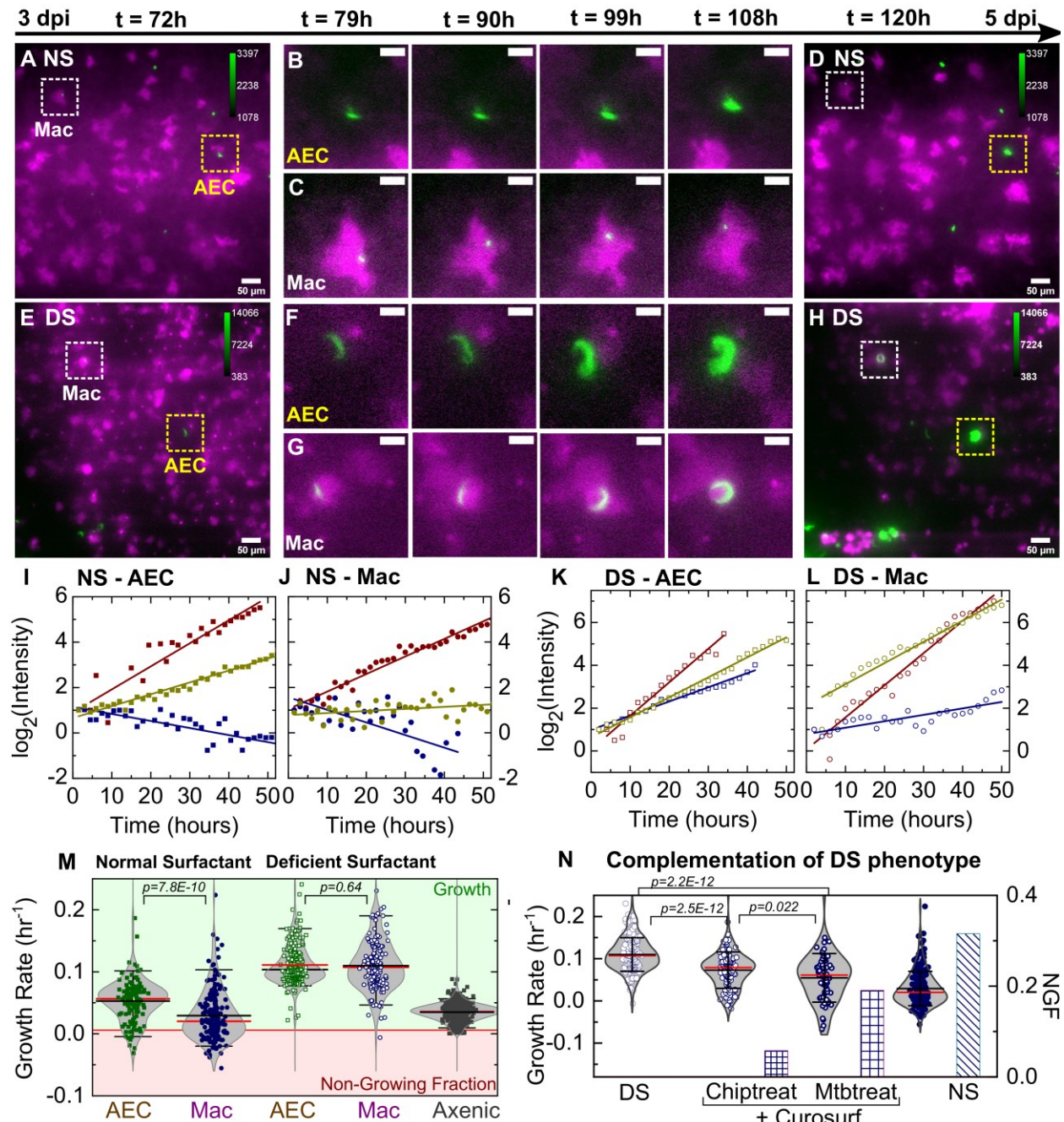
584   test.

585

586

25

Fig. 2. Surfactant deficiency results in uncontrolled intracellular growth of Mtb. Snapshots

from live-cell imaging at 1.5- to 2.0-hour intervals between 3-5 days post-infection (dpi) in NS

(**A-D**) and DS (**E-H**) LoCs. Macrophages are false-colored magenta; Mtb is false-colored green.

The calibration bar (inset in **A, D, E, H**) indicates the absolute intensities in the Mtb channel, the

592   scales were chosen to achieve a similar saturation level in the images across surfactant conditions.

593   Representative examples of infected AEC (yellow boxes) and macrophage (white boxes) are

594   highlighted, and zooms (**B, C, F, G**) reveal growth in both cell types over this period. Scale bar,

595   10 μm. (**I, J**) Plots of the logarithm of total fluorescence intensity over time confirm exponential

596   Mtb growth for representative infections in AECs (**I, K**) and macrophages (**J, L**) under NS and

597   DS conditions, respectively. In each case, an intracellular microcolony with growth rate close to

598   the population maximum (red), median (yellow), and minimum (blue) is shown. The growth rate

599   is the gradient of the linear fit. (**M**) Scatter plots of Mtb growth rates in AECs (n=122 for NS,

600   n=219 for DS) and macrophages (n=185 for NS, n=122 for DS). Growth is significantly slower in

601   macrophages than AECs in NS conditions ($P = 7.8E-8$) but not in DS conditions ($P = 0.64$), and

602   is more heterogenous in both conditions compared to single-cell Mtb growth rate data from axenic

603   microfluidic cultures. The green- and red-shaded regions indicate growing bacteria and the non-

604   growing fraction (NGF), respectively. (**N**) Uncontrolled growth in DS conditions can be rescued

605   by exogenous administration of Curosurf^{TM}. Scatter plots represent Mtb growth rates in a DS LoC

606   treated with Curosurf^{TM} ('Chiptreat') or infected with Mtb preincubated with Curosurf^{TM}

607   ('Mtbtreat'). Data from DS and NS LoC infections (no Curosurf^{TM}) are included for comparison.

608   Growth attenuation for both treatments is significant relative to DS conditions as reflected by the

609   average growth rate and the size of the NGF (n=122 for DS, n=121 for Chiptreat, $P = 2.5E-12$

610   n=63 for Mtbtreat, $P = 2.2E-12$, and n=122 for DS). *P*-values were calculated using a Kruskal-
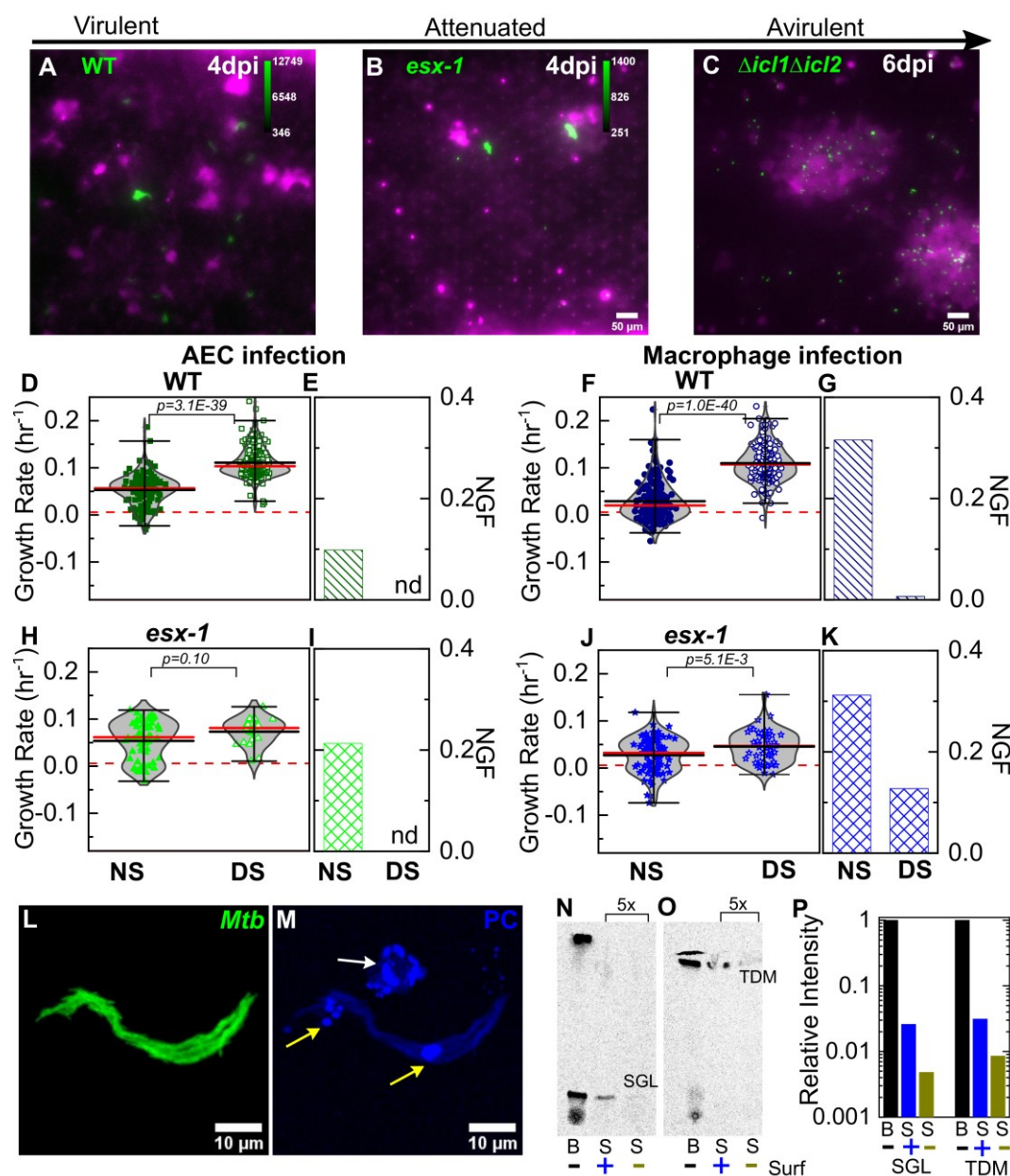
611   Wallis one-way ANOVA test.

612

Fig. 3. Surfactant depletes virulence factors on the bacterial cell surface. Snapshots from live-cell imaging in DS conditions at 4 days post-infection for (**A**) wild-type Mtb, (**B**) an attenuated ESX-1 deficient strain (*esx-1*), and (**C**) at 6 days post-infection for the avirulent Δ*icl1* Δ*icl2* strain infected at a higher inoculum. The calibration bar (inset in **A-C**) indicates the corresponding absolute intensities in the Mtb channel for a direct comparison across strains. Growth of the ESX-1 deficient strain is attenuated relative to wild-type Mtb (~10 fold decrease in intensity) and the

620   Δ*icl1*Δ*icl2* strain is unable to grow. Scatter plots indicate Mtb growth rate in individual AECs (**D,**

621   **H**) and macrophages (**F, J**) and bar graphs indicate the non-growing fraction (NGF) of bacteria for

622   infected AECs **(E, I)** and macrophages **(G, K)** in normal surfactant (NS) and deficient surfactant

623   (DS) conditions for wild-type and ESX-1 deficient strains. 'nd', not detected. Each dataset was

624   fitted with a non-parametric kernel density estimation characterised by the mean (black) and

625   median (red) values and whiskers represent the 1-99 percentile interval. For wild-type Mtb, DS

626   conditions significantly increase growth rates and lower the NGF in both AECs (**D, E**) (n=122 for

627   NS, n=219 for DS, P=3.1E-39) and macrophages (**F, G**) (n=185 for NS, n=122 for DS, P=1.0E-

628   40). For the ESX-1 deficient strain, differences between NS and DS conditions are not significant

629   in AECs (**E**) (n=61 for NS, n=25 for DS, P=0.10); for macrophage infection, differences are

630   statistically significant (**J**) (n=93 for NS, n=55 for DS, P=5.1E-3), but a significant number of

631   bacteria remain non-growing in DS conditions (**K**). (**L, M**) Maximum intensity projections of an

632   aggregate of fluorescent Mtb (false-colored green, (**L**)) after incubation with a 1% solution of

633   Curosurf^{TM} labelled with 10% v/v TopFluor-Phosphatidylcholine (PC) (false-colored blue, (**M**)).

634   PC is incorporated into surfactant micelles (indicated by arrows in (**M**)), which also associate with

635   and coat the bacteria (yellow arrows). (**N, O**) Thin layer chromatography of total free lipid

636   extracted from wild-type Mtb (B) or bacterial culture supernatants (S) with (+) or without (-)

637   Curosurf^{TM} pre-treatment. The latter two samples were spotted 5x in excess. Running solvents are

638   (**N**) 90:10:1 chloroform: methanol: water to identify sulfoglycolipids (SGL), and (**O**) 80:20:2

639   chloroform: methanol: ammonium hydroxide to identify trehalose dimycolate (TDM). (**P**)

640   Intensities of the SGL and TDM bands for the three samples in (**N, O**) are plotted relative to that

641   for the bacterial sample without surfactant treatment (labelled 'B'). P-values were calculated using

642   a Kruskal-Wallis one-way ANOVA test.